STRUCTURE DETERMINATION OF A QUINOLINONE ALKALOID FROM THE FUNGUS *ASPERGILLUS NIDULANS* USING 1D AND 2D-NMR ANALYSIS

A Thesis

Presented to the Faculty of the Graduate School

of Cornell University

In Partial Fulfillment of the Requirements for the Degree of

Master of Science

by

Juniper Thang Wenbin

August 2020

ABSTRACT

Nuclear Magnetic Resonance (NMR) spectroscopy techniques have been used rigorously by analytical chemists to determine the molecular structure of natural products derived from plants, bacteria and fungi for purposes such as drug discovery and genome mining. In this work, Mass Spectroscopy (MS), Infrared Spectroscopy (IR) and 1D and 2D NMR techniques were employed to determine the full structure of a quinolinone alkaloid (compound 1) derived from the fungus *Aspergillus Nidulans*. The final structure obtained was a hydroxylated quinolinone alkaloid derivative with a 2,2,4-trimethyl-4-vinyl-3-oxabicyclo[3.1.0]hexane moiety attached. Since the lack of protonation on certain carbons prevented NOESY NMR from determining stereochemistry of all stereocenters, Residual Dipolar Couplings (RDCs) and Electronic Circular Dichroism (ECD) spectroscopy can be utilized in the future to ascertain the absolute stereochemistry of the quinolinone alkaloid.

BIOGRAPHICAL SKETCH

Juniper Thang Wenbin graduated with a Bachelor of Science (Specialization – Organic Chemistry) from the National University of Singapore in 2019. At present, she is pursuing her Master's in Chemistry & Chemical Biology at Cornell University, which is scheduled for completion in 2020. Her interests include the use of Chemical Biology techniques and single molecule studies to study anti-cancer and anti-viral drugs. Following completion of her masters, Juniper will be pursuing a teaching career in Chemistry in Singapore.

ACKNOWLEDGMENTS

I would like to express my sincere gratitude to my student advisor Associate Professor David B. Zax for coordinating the Chemistry Master's program and his constant advice throughout the year. Dr. Zax's input and guidance were instrumental in the writing of this thesis. I am also grateful for Professor Frank C. Schroeder's spectroscopy class, where I learnt valuable NMR and MS theory and techniques. I would also like to thank Professor H. Floyd Davis for being the secondary member in my special committee and for attending my oral defense.

Lastly, I would like to thank my family, friends and classmates who helped me throughout my years of education, by being there for me physically and emotionally.

TABLE OF CONTENTS

Introduction

For hundreds of years, researchers have been studying natural products from fungi for their anti-microbial[1], analgesic, anti-cancer properties[2] and more. One family of such products are the alkaloids – organic molecules containing basic nitrogen atoms, which are used medically for their anti-malarial, anti-asthma, anti-arrhythmic and anti-cancer activities[3-4]. For example, cytotoxic alkaloids and antibiotics have been derived from the marine fungus *Aspergillus sydowi*[5], and isoquinoline alkaloids from the fungus *Penicillium Spathulatum* have proven to exhibit antibacterial properties[6]. However, despite its potential as an excellent source of pharmaceuticals, it is estimated that only ~5% of fungi's biodiversity[7] has been exploited as natural products from bacteria and plants are typically easier to procure. For example, fungal biosynthetic gene clusters may remain silent under laboratory culture conditions[8], keeping the expression of genes and corresponding secondary metabolites cryptic. As such, more attention should be focused on characterizing unknown natural products from fungi, increasing chances of novel drug discovery.

In this work, the structure of a quinolinone alkaloid extracted from the fungus *Aspergillus Nidulans* was elucidated through mass spectrometry, infrared spectroscopy and NMR techniques. The fungus model *Aspergillus nidulans* has been studied extensively for natural products such as bioactive isoindolinone alkaloids[9] and for genome mining purposes such as characterizing polyketide biosynthetic gene clusters[10]. Anti-cancer products such as the anti-proliferative polyketide asperfuranone[11] was also derived from the fungus *Aspergillus Nidulans.* Upon elucidating the structure of this quinolinone alkaloid, the molecule can then be modified to improve its anti-cancer/ anti-bacterial performance in vitro and in

vivo. Elucidation of the structure will also allow for analysis of specific binding interactions at the drug's potential target site.

Methods

It should be noted that the various spectra of compound 1 (Fig. S1- S10) were obtained from the work "Prenylated quinolinone alkaloids and prenylated isoindolinone alkaloids form the fungus *Aspergillus Nidulans*" by Y. Zhang et al. and solved independently. It was originally planned for a given unknown compound to be analyzed by the student in the lab, but this was cancelled due to COVID-19 lab-entry restrictions.

Mass Spectroscopy

HRESIMS (High-Resolution Electrospray Ionization Mass Spectroscopy) was first used to determine the molecular mass of the alkaloid. ESI is a soft ionization technique which ionizes the analyte in solution into intact molecular gaseous ions.[12]. The ions are separated based on their mass/charge ratio and the number of ions representing each mass/charge unit is recorded in the spectrum. ESI is termed a soft ionization technique as it rarely causes fragmentation upon ionization, hence producing the molecular ion signal consistently[12]. High-resolution MS allows for m/z value to be determined to up to 4 or 5 decimal places, hence allowing precision in determining molecular formula.

The ESI mechanism is shown in Fig 1:

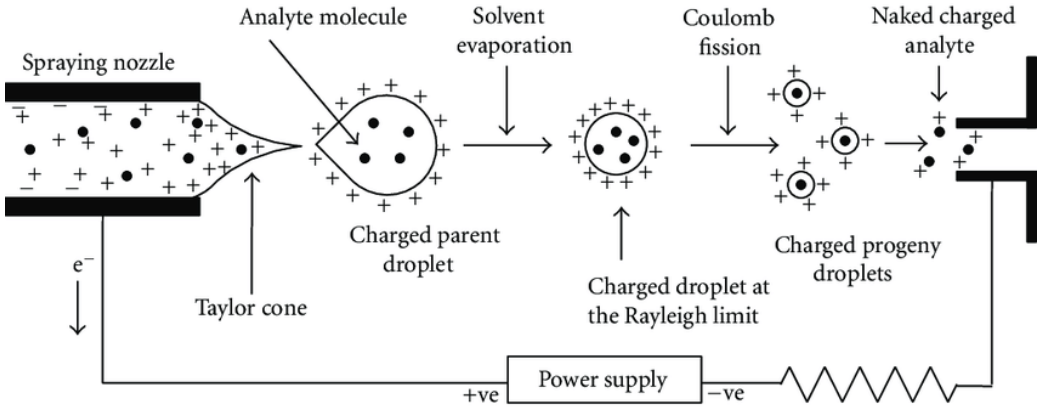

Fig 1. Electrospray Ionization Mechanism[13]

The high voltage applied causes electrochemical redox reactions to occur to the solvent, releasing producing positive and negative ions which accumulate in the spraying nozzle. For this to happen, solvents that easily undergo electrochemical reactions should be used. The chosen solvent must also be volatile as extensive solvent evaporation is needed to form smaller charged droplets of higher charge density, which can then undergo coulomb fission at the Rayleigh limit to form charged progeny droplets to be detected and analyzed[13]. Therefore, common solvents used include the volatile and polar methanol and acetonitrile.

Infrared Spectroscopy (IR)

Infrared Spectroscopy (IR) was employed to characterize prominent functional groups. In IR spectroscopy, infrared radiation from 4000cm^{-1} to 400cm^{-1} is absorbed and converted by organic molecules into energy of molecular vibration, which consists of stretching and bending vibrations. For harmonic oscillators, the frequency of absorption depends on both the mass of the molecule and force constants acting on the bonds ($v = \frac{1}{2\pi c}\sqrt{\frac{K}{\mu}}$), where μ is reduced mass of the molecule

and *K* is force constant[14]. Therefore, stronger bonds ($sp > sp^2 > sp^3$) such as bonds to hydrogen (O-H, N-H, C-H), triple bonds (C≡C, C≡N) and double bonds tend to be of higher frequency while single bonds (C-O, C-F, C-Cl) tend to be of lower frequency.

In this work, some frequencies that would be useful would be those of O-H (broad peak at 4000 – 3000 cm^{-1}), C-O (1300 – 1000cm^{-1}), aromatic C=C (sp^2 C-H occurs at values greater than 3000cm^{-1}) and amides (C=O at 1680 – 1630cm^{-1} and one band at 3300cm^{-1} for secondary N-H)[14]. While IR spectroscopy may be useful for the initial stages of structure elucidation, one should avoid interpreting every single peak and instead use the information derived as a rough gauge of functional groups present. In reality, bending modes are rarely harmonic. Therefore, we cannot simply attribute a peak observed at a certain frequency to a specific bond, unless the peak is of a very distinguishable or isolated frequency.

For example, a broad band at ~3300 – 3000cm^{-1} could represent either a hydroxyl or an amine group; and there is rarely enough information in an IR spectrum to determine which is truly present. Distinctions can be made with greater ease when a vibration mode has significant intensity. For example, the C=O stretch for an aliphatic aldehyde appears in the range 1740-1725cm^{-1} at very strong intensity, making it easily distinguishable. Due to the ambiguities present in IR analysis, most of our effort was invested in the use of NMR to gather more information about the connectivity of the hydrocarbon skeleton.

1D NMR Analysis

^{1}H-NMR analysis gives a clearer picture of the functional groups in the molecule. In ^{1}H-NMR, there are four main components for analysis – chemical shift, multiplicity, peak integral and coupling constants. The chemical shift suggests identities of possible functional groups or positions of heteroatoms. The greater the chemical shift, the less shielded the proton is, suggesting the presence of a neighboring electronegative heteroatom or possible anisotropy. For example, R-O-CH_3 and R-CH_3 may present chemical shifts at 3.2-3.8ppm and 0.7-1.3ppm[15] respectively, as the former methyl proton is less shielded. Aromatic protons tend to cause signals at 6.5-8.0ppm[15] as they are de-shielded by the large anisotropic field generated by electrons in the ring's π system. The same anisotropic effect in double bonds also cause vinylic hydrogens to have chemical shifts of 4.5-6.5ppm.

Peak multiplicities tell us information about coupled protons. A set of non-equivalent protons splits the signal of a neighboring proton into (n+1) peaks. As a result, the methyl protons of RCH_2CH_3 appear as a triplet and the methine in $ROCH_2CHCH_2CO$ would likely be a triplet of triplets (if first-order multiplet). Singlets are also very useful in analysis, since they represent isolated protons e.g. The methyl of R-O-CH_3 would produce a singlet. The peak integral, or the area under an NMR signal is proportional to the number of absorbing protons, and hence the integral 5.11 of the peak at 7.26ppm indicates 5 absorbing protons.

It should be noted that the (n+1) rule only applies to first-order multiplets. The first-order splitting pattern occurs when the chemical shift difference in Hz between two coupled peaks is significantly larger than the J coupling constant ($\nu_A - \nu_X >> J_{AX}$),

resulting in the AX system shown in Figure 2. Truly first-order multiplets can be recognized by their centro-symmetry.

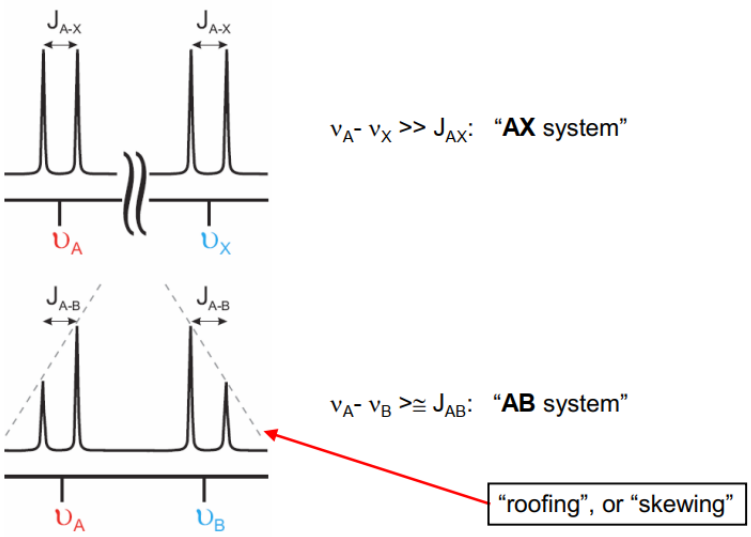

Fig 2. First-order (AX system) and higher-order (AB system) splitting patterns[16]

Higher-order splitting patterns occur when the chemical shift difference is only slightly greater or equal to the J coupling constant ($\nu_A - \nu_X >= J_{AX}$) i.e. chemical shits of two coupled protons are too close, causing the roofing effect (Fig. 2). The roofing pattern exhibits taller inner peaks and shorter outer peaks. Using higher field strength may allow for a second-order multiplet to resolve into a first-order multiplet.

Lastly, different coupled pairs of protons exhibit different coupling constants. A trans pair of vinylic protons produce a coupling constant of 11-18Hz while a cis pair produces a coupling constant of 6-15Hz[14]. Figure 3 shows zoomed-in screenshots of the COSY spectrum of vinylic protons in Roquefortine C.

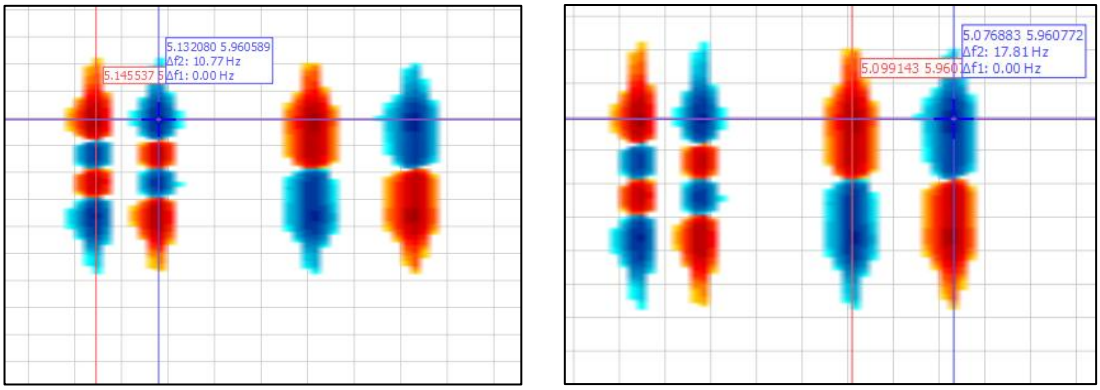

Fig 3. Zoomed-in screenshots of the cis pair (left) and trans pair (right) of vinylic protons in the COSY spectrum of Roquefortine C

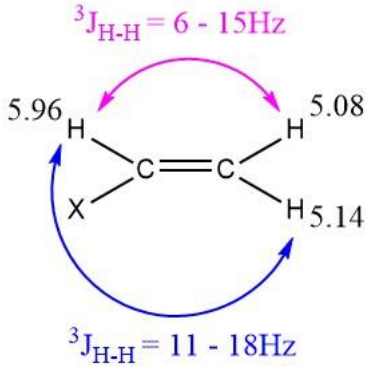

Fig 4. Expected coupling constants for a cis pair and trans pair of vinylic protons

As shown in Fig 3, the cis pair of protons exhibited a coupling constant $J_{H5.14\text{-}H5.96}$ = 10.77Hz, which is within the range of a cis pair of vinylic protons (J = 6-15Hz). Likewise, the trans pair of protons exhibited $J_{H5.08\text{-}H5.96}$ = 17.81Hz which is within the expected range of a trans pair of vinylic protons (J = 11-18Hz). This allows for easy assigning of chemical shifts to the respective vinylic protons.

An ortho pair of aromatic protons results in a coupling constant of 6-10Hz while the two vinylic protons in a cyclohexene ring results in a coupling constant of 8-11Hz.

^{3}J and ^{2}J coupling values are usually the largest, followed by long-range couplings such as ^{4}J (0-3Hz)[15]. While ^{4}J couplings are usually <0.5Hz, they can reach up to 3Hz when there are intervening π bonds.

To clarify and extend the information provided by the ^{1}H spectrum, the ^{13}C-NMR and DEPT spectrum were utilized. The ^{13}C-NMR displays two important features – the number of signals and their chemical shifts. The resonances due to ^{13}C nuclei are split by neighboring H atoms, but these splitting patterns complicate the spectrum and make it challenging to interpret. Therefore, ^{13}C-NMR spectra are usually decoupled. This means applying a continuous second radio frequency signal of broad frequency range to excite all the H nuclei, eliminating all ^{13}C-^{1}H coupling patterns. ^{13}C-^{13}C couplings are also negligible and usually do not show up on the spectrum as only ~1.1% of naturally occurring C atoms have ^{13}C nuclei. As a result, the spectrum is reduced to single peaks for ease of interpretation. From the chemical shifts, we can identify functional groups e.g. aldehydes and ketones are present at 185-220ppm while acids, esters, amides and anhydrides are present at 155-185ppm[15].

By comparing the ^{13}C-NMR to the DEPT-90 and DEPT-135, one can differentiate quaternary, methine, methylene and methyl carbons (see Fig. 5) Quaternary carbons show signals in only the ^{13}C-NMR, methine carbons show positive peaks in all three spectra, methylene carbons show negative peaks in DEPT-135 and methyl carbons show positive peaks in DEPT-135. Neither the methylene nor methyl carbons appear in the DEPT-90, as illustrated in figure 5 below.

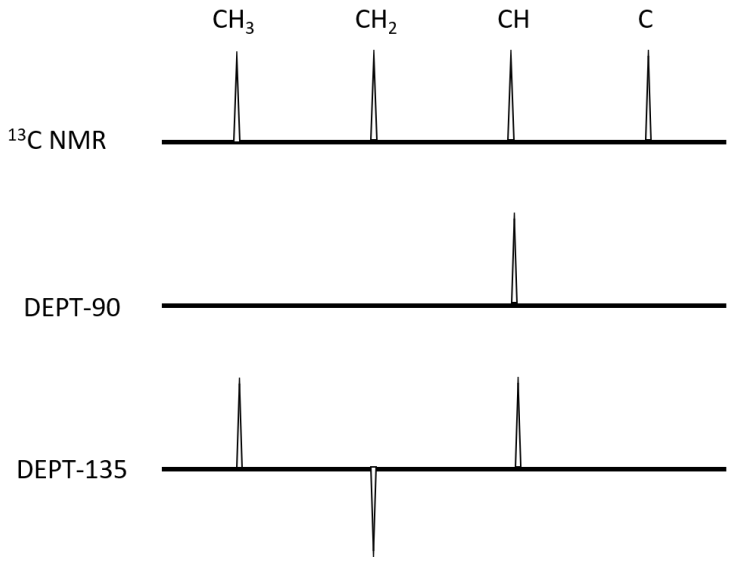

Fig 5. Comparison of signals in ^{13}C-NMR, DEPT-90 and DEPT-135. The ^{13}C NMR shows all carbon peaks, the DEPT-90 shows only methine peaks and the DEPT-135 shows positive methyl and methine but negative methylene peaks.

A proton tip angle, θ, is the key to what differentiates DEPT-45, DEPT-90 and DEPT-135. DEPT-45, DEPT-90 and DEPT-135 employ a proton tip angle of 45°, 90° and 135° respectively. To understand how the proton tip angle is chosen to result in display of the desired carbon multiplicities (methine, methylene or methyl), one must first understand how spectral editing with INEPT works.

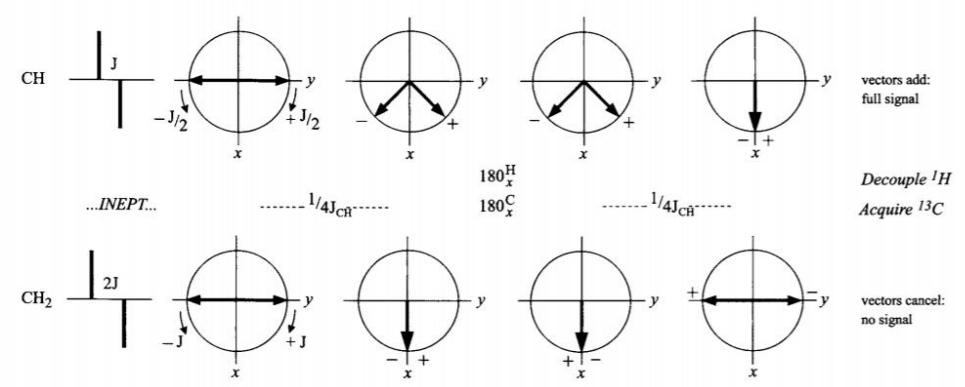

Fig 6. Refocused-INEPT visualized by the vector model. A Δ_2 period of 1/2J refocuses the doublets (CH), but causes triplets and quartets (CH_2 and CH_3) to be anti-phase (bottom row) [16]

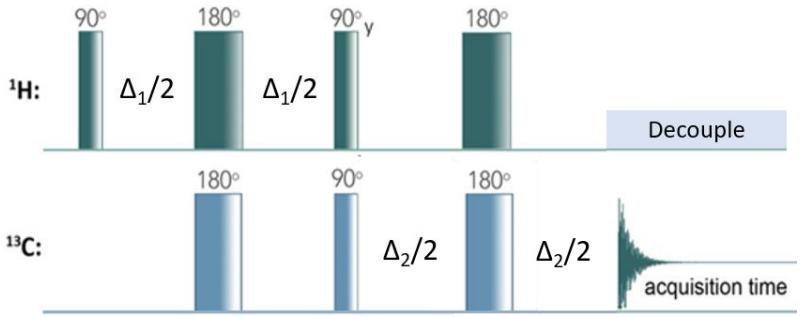

Fig 7. The refocused INEPT pulse sequence

Using a Δ_2 period of 1/2J in the refocused-INEPT sequence (Fig. 7) causes triplets and quartets to be anti-phase (Fig. 6), hence resulting in a spectrum with only methine peaks present. Using different Δ_2 can hence result in spectra with the methylene and methyl peaks as well. The proton tip angle (θ) can be defined as $\theta = 180J\Delta_2$ whereby the signal intensities (I) in the decoupled experiment are: [16]

$$\text{CH: } I \propto \sin\theta$$

$$CH_2\text{: } I \propto 2\sin\theta\cos\theta$$

$$CH_3\text{: } I \propto 3\sin\theta\cos^2\theta$$

which are plotted on the graph below:

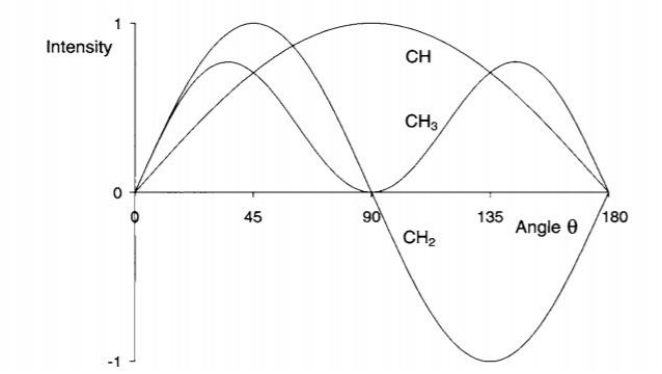

Figure 8. Plot of intensity against delay period Δ_2 ($\theta = 180J\Delta_2$) [16]

As shown in figure 8, $\theta = 90°$ which is allowed by a Δ_2 period of 1/2J will cause only methine peaks to be present, which is essentially the basis of DEPT-90. $\theta = 45°$ allows for methine, methylene and methyl peaks to be shown while $\theta = 135°$ (DEPT-135) allows for methine and methyl peaks to be displayed as positive signals and methylene peaks to be negative signals. The only difference between INEPT and DEPT is that with DEPT, editing is achieved through the angle θ and is independent of the J coupling constant. The Δ_2 period in INEPT, however, is still chosen based on the J coupling constant ($\theta = 180J\Delta_2$).

2D NMR Analysis

2D NMR analysis plays the most prominent role in structure elucidation and sometimes can be the sole technique needed to determine structure, even in the absence of information from MS, IR or 1D NMR. Typically, HSQC (Heteronuclear Single Quantum Correlation) analysis will be carried out first.

The HSQC is a 2D experiment whereby magnetization is transferred between directly bonded ^{1}H and ^{13}C. The resulting 2D chemical shift correlation map shows crosspeaks from $^{1}J_{CH}$ couplings, revealing which proton is directly bonded to which carbon.

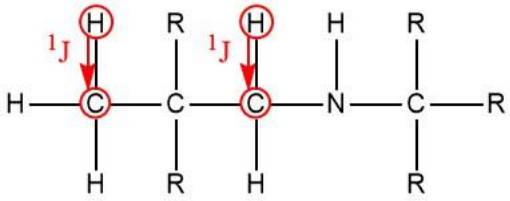

Fig 9. $^{1}J_{CH}$ couplings obtained from HSQC

With HSQC, we can assign all carbons to their attached protons with the exception of quaternary carbons, since they do not carry protons. HSQC in conjunction with ^{1}H-NMR can reveal the chemical shift assignments of methyl, methylene and methine carbons.

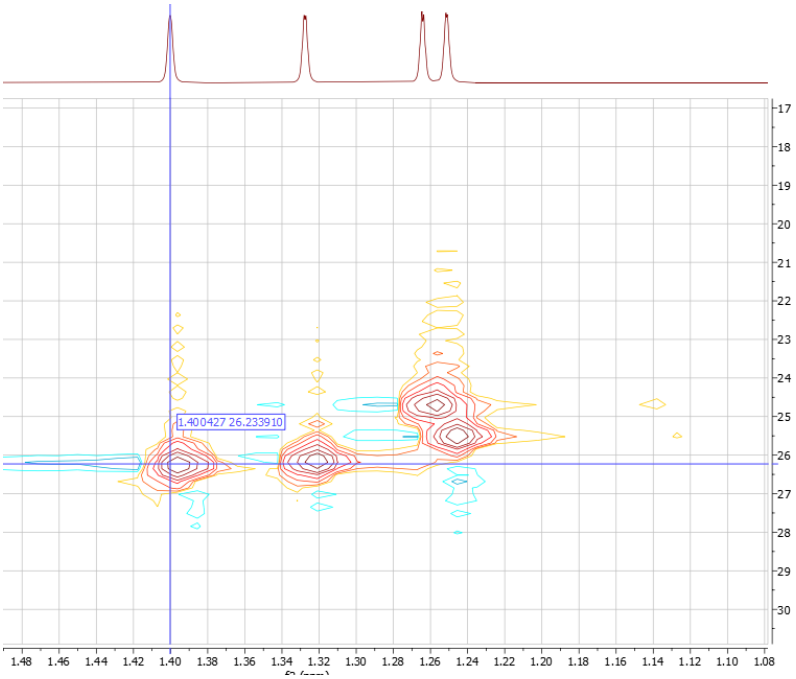

Fig 10. HSQC of an unknown sugar with focus on a methyl group crosspeak

In this HSQC spectrum of an unknown sugar, a crosspeak is present at the coordinates (1.400427, 26.233910), showing that C (δ = 26.2ppm) is attached to H (δ = 1.40ppm). However, we do not yet know the number of protons the H signal at 1.40ppm represents. From the ^{1}H-NMR, H (δ = 1.40ppm) was shown to be a likely methyl group due to its integral of ~3 and strong intensity. Therefore, ^{1}H-NMR and HSQC can be used together to show that C (δ = 26.2ppm) represents a methyl group.

The following shows the HSQC pulse sequence:

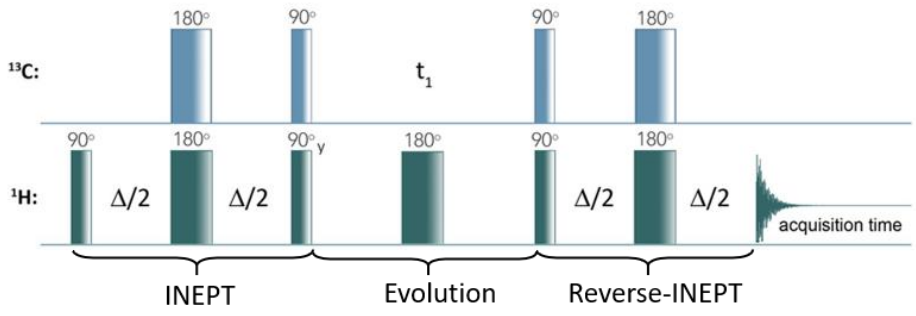

Fig 11. HSQC pulse sequence

While understanding of pulse sequences is not essential in reading HSQC spectra and elucidating structures, comprehending pulse sequences will allow us to modify the sequence to obtain desired spectra; or modify parameters such as evolution time (t_1) or acquisition time (at) to obtain desired resolution or signal-to-noise ratio.

The pulse sequence above can be de-constructed into the preparation, evolution and mixing phases. The preparation phase is an INEPT (Insensitive nuclei enhancement by polarization transfer) sequence which is employed to improve sensitivity by polarization transfer from the sensitive ^{1}H nuclei to the insensitive ^{13}C nuclei. In Figure 9, the initial INEPT sequence transfers polarization from ^{1}H to ^{13}C via $^{1}J_{CH}$ coupling. The variable evolution period (t_1) allows for anti-phase ^{13}C magnetization

to evolve under the effect of C chemical shift. The ^{1}H 180° pulse in the middle of the evolution period refocuses ^{1}H-^{13}C couplings, eliminating the effects of coupling while maintaining the effects of chemical shift. Next, a reverse INEPT is engaged to convert C magnetization into in-phase ^{1}H magnetization. Lastly, proton acquisition (mixing phase) is carried out with C decoupling.

Next, COSY (Correlation Spectroscopy) is a ^{1}H-^{1}H two-dimensional experiment used to identify protons coupled (and create cross-peaks) to any and all other ^{1}H chemical environments within a few bonds—which are traversed via the J couplings between those chemical environments.

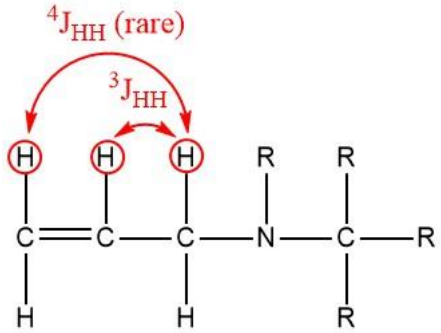

Fig 12. $^{3}J_{HH}$ and $^{4}J_{HH}$ couplings obtained from COSY

While the one-dimensional spectrum reveals similar information in the multiplet patterns, COSY is used to identify not just how many but which other sites are typically within two or three bonds. The 1D ^{1}H spectrum may also be challenging to interpret due to extensive second order coupling and overlapping multiplets. As the presence of crosspeaks depend on the size of the J couplings, these H-H couplings may in unusual cases show four or five bond couplings, as in some allylic systems (Allylic ^{4}J coupling constants can reach up to 3Hz or greater). With COSY, we can identify entire spin systems in the molecule, breaking the molecule into

conceivable fragments. Dqf-COSY (double quantum-filled COSY) is another form of COSY that can be used to remove severe tailings in diagonal peaks[16], thereby improving quality of the spectrum.

Fig. 3 is an example of COSY analysis. From HSQC, one would have deduced that both $H_{5.08}$ and $H_{5.14}$ are attached to the same carbon. Since the COSY spectrum shows couplings $H_{5.14} \rightarrow H_{5.96}$ and $H_{5.08} \rightarrow H_{5.96}$, we know that $H_{5.96}$ is a neighbor of both $H_{5.08}$ and $H_{5.14}$. Since the COSY spectrum does not show any other couplings involving these three protons, one can deduce that these protons are likely isolated from other parts of the molecule by a heteroatom or quaternary carbon (represented by X). With this information, the fragment in Fig. 4 can be conceived.

The COSY pulse sequence is shown in the following:

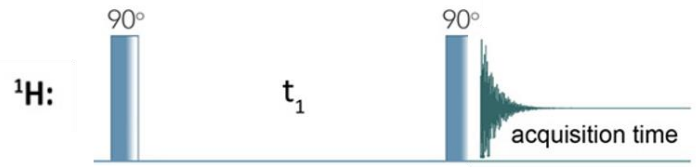

Figure 13. COSY pulse sequence

The COSY sequence is a simple two-pulse sequence with an evolution period in between. During t_1, evolution will take place under the effect of both coupling and chemical shift. This is followed by a measurement period (acquisition time).

HMBC (Heteronuclear Multiple Bond Correlation) is a ^{1}H-^{13}C two-dimensional experiment used to identify long-range ^{1}H-heteronuclei (usually ^{13}C) couplings by taking advantage of the higher sensitivity of proton detection. Using HMBC, we can identify two or three bond C-H couplings (occasionally weaker four or five bond couplings), whereby correlation between C and H passes over heteroatoms and

quaternary carbons. As shown in figure 14, the ^{3}J coupling on the right passes over the nitrogen heteroatom and the ^{3}J coupling on the left passes over a quaternary carbon.

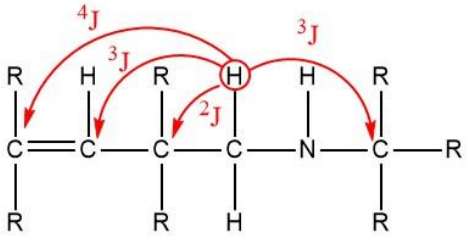

Figure 14. Possible HMBC ^{1}H-^{13}C correlations

This allows for connection of the COSY-derived fragments, and to locate where the quaternary C sites belong, to form an initial guess of the chemical connectivity of the molecule. For example, fragments identified via the COSY experiments may be separated by a heteroatom or quaternary carbon and therefore have no sufficiently large ^{1}H-^{1}H J couplings to appear as near-neighbors in the bonding pattern, but HMBC will detect that long-range connection.

The HMBC pulse sequence is essentially the HSQC sequence but tuned to detect correlations with small couplings. This discussion will explain how HMBC is selective for long-range couplings.

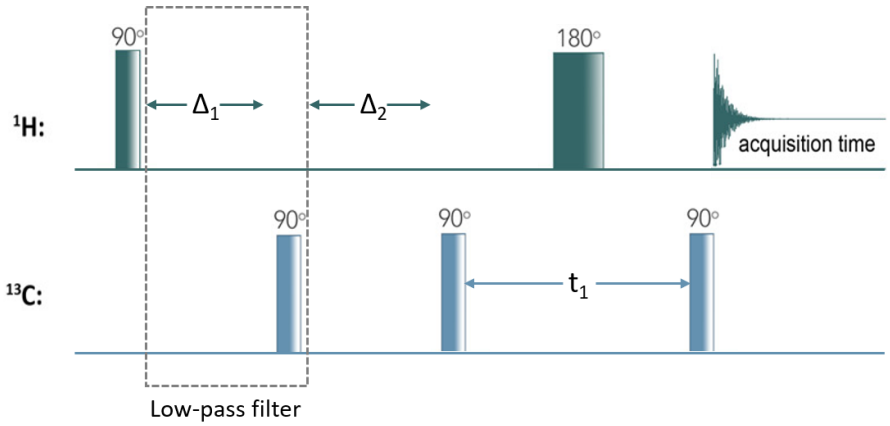

Figure 15. HMBC pulse sequence with low-pass filter

In order to allow for small long-range ^{1}H-^{13}C couplings to evolve, the Δ_2 period of preparation must be sufficiently long. Long range ^{1}H-^{13}C couplings (~0.5Hz) are at least an order of magnitude smaller than ^{1}J couplings (<5Hz), thus requiring Δ_2 to be at least 100ms. However, this longer preparation period may be a multiple of the appropriate setting for ^{1}J couplings, thus allowing one-bond ^{1}H-^{13}C couplings to appear like in HSQC. This is undesired as it makes it difficult to differentiate crosspeaks due to one-bond couplings and crosspeaks due to long-range couplings on the HMBC spectrum. As a result, a low-pass J-filter (Fig. 15) is employed to eliminate ^{1}J couplings. The low-pass filter allows for couplings of lower J (long-range coupling) to "pass through", while cancelling out couplings that exceed a chosen cut-off value (chosen to be the one-bond coupling constant value in this case). This is the main mechanism that differentiates HMBC from HSQC. Other than that, pulsed field gradients can also be added to the HMBC pulse sequence to eliminate satellite peaks from parent ^{1}H-^{12}C couplings.

However, none of these techniques will help with detection of stereochemistry, hence the need for the NOESY (Nuclear Overhauser Effect Spectroscopy) experiment. A cross-peak on the NOESY spectrum indicates that two protons are close to one another in space ($\leq$5Å) and are hence likely co-facial. It is important to note that absence of a NOESY peak, however, is not sufficient to confirm that two protons are anti-facial.

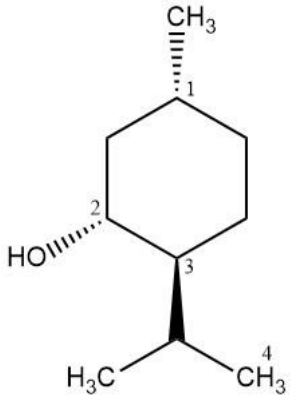

Figure 16. (-)-Menthol

For example, for the (-)-Menthol molecule in Fig. 16, one would expect to obtain NOESY crosspeaks due to H1-H2 coupling as they are co-facial. H2 and H3 are anti-facial and will not couple through space, hence one would not expect a crosspeak to appear. However, the absence of a H2-H3 crosspeak is not enough evidence to confirm that H2 and H3 are anti-facial. One would instead look for a H2-H4 crosspeak to determine the stereochemistry of the isopropyl group relative to the OH group.

In the following, we will attempt to demonstrate the process of structure determination on the molecule (compound 1) isolated from the fungus *Aspergillus Nidulans* with reference to the spectra (Fig. S1-S10) provided below.

Results & Discussion

HRESIMS analysis

The HRESIMS spectrum displays its highest intensity peak at 458.1945 m/z with a charge of +1, thus accounting for the molecular formula $C_{26}H_{29}NO_5Na$[1]. The possibility of a di-cation was ruled out as that would imply a molecular formula of 916 which is unlikely for a molecule with at least 25 carbons (see ^{13}C-NMR results). The degree of unsaturation was hence calculated to be 13.

There are a few reasons why sodium or potassium might be present in the sample. Typical positively charged adducts include $[M+H]^+$, $[M+Na]^+$, $[M+K]^+$, $[M+NH_4]^+$ and typical negatively charged adducts include $[M+H]^-$, $[M+Cl]^-$, $[M+Br]^-$ and $[M+CH_3CO_2]^-$. However, the most commonly observed metal adducts in ESI MS are the sodium and potassium adducts. As mentioned in the methods section, common solvents used in ESI include methanol and acetonitrile, which facilitate fast solvent evaporation. In such solvents, sodium and potassium are bound to be found in trace amounts, even in almost pure (99.9%) pure acetonitrile. Na and K can also leech out of glassware as various salts are used in the glass manufacturing process and dissolve in the presence of polar solvents[17]. They can also come from the experimenter if not careful, or come in high concentrations in biological samples[17].

While it was possible no metal adduct was formed at all, the mass 458.1945 revealed highly improbable molecular formulae such as $C_9H_{20}N_{19}O_4$ and $C_{10}H_{26}N_{12}O_9$, which is again in disagreement with the ^{13}C-NMR results (at least 25 carbons) and have unrealistic numbers of nitrogen atoms (relative to carbon atoms). While another potential molecular formula ($C_{25}H_{23}N_8Na$) was considered, ^{13}C NMR showed a

[1] This molecular formula was obtained via ChemCalc.

distinct peak at 168.93ppm, suggesting the presence of an ester, amide or carboxylic acid, thus being rejected for its absence of oxygen atoms. Potassium adducts were also considered. Potential molecular formulae with potassium (K) atoms include $C_{23}H_{33}KNO_6$ and $C_{22}H_{27}KN_8O$, but they also had insufficient numbers of carbons.

^{1}H NMR analysis

The presence of six protons in the region above 7ppm suggests the possibility of six or more aromatic protons, five (δ = 7.26ppm) of which are likely to be on the same aromatic ring, while H (δ = 7.37) lies on a separate aromatic ring, split into a doublet by a neighboring proton. H (δ = 6.38) and H (δ = 6.85) represents a potential double bond, but they could also represent aromatic protons. Three methyl groups (δ = 1.29, 1.2, 1.32), a methoxy (δ = 3.54) and a methine (δ = 3.64) adjacent to an oxygen (R-O-CH-) are present. Methyl groups often present themselves at 0.7-1.4ppm, and are typically recognizable as tall singlets, doublets or triplets depending on their coupling with neighboring protons. In this work, they all exhibit integrals of ~3 and are all singlets, indicating that they are isolated methyl groups. The protons at very low chemical shifts (δ = 0.51, 0.45) may indicate a cyclopropane group, since protons in cyclopropane are highly shielded[18].

The OH and NH peaks are absent from the ^{1}H spectrum (Fig. S2). This may be because proton signals from OH or NH groups are usually broad due to rapid exchange with protons in the solvent, and hence may not have strong enough intensity to appear. Otherwise, one may typically observe OH peaks at 0.5-5.0ppm and NH peaks at 0.5-4.0ppm, depending on many factors such as temperature, acidity, amount of hydrogen bonding and solvent. For example, decreasing temperature may reduce rate of proton exchange, resulting in relatively sharp OH

peaks. More hydrogen bonding between the hydroxyl groups may also reduce chances of proton exchange and result in sharper peaks. In this work, the absence of OH and NH peaks is likely due to exchange with the deuterated solvent CD_3OD, creating OD and ND groups which may have peaks that are out of the range of the spectrum.

^{13}C NMR and DEPT analysis

As aforementioned, the ^{13}C NMR peak at 168.93ppm indicates the presence of an ester, amide or carboxylic acid. However, absence of a ^{1}H-NMR peak in the 11-12ppm range rules out a carboxylic acid group[15]. The cluster of carbons from 108.14 to 156.74ppm may represent aromatic carbons, some with higher chemical shifts (δ = 156.74, 140.41) that may be attributed to neighboring heteroatoms. C (δ = 59.19) indicates a likely R_3C-O- group and the cluster of carbons from 26.24 to 29.69ppm are likely to contain some methyl group carbons. The DEPT spectrum shows only one methylene carbon (δ = 6.57ppm) and by comparing the DEPT to the ^{13}C-NMR spectrum, the quaternary carbons (δ = 168.93, 156.74, 140.41, 122.34, 122.68, 84.35, 83.18, 80.15) can be identified. A total of 23 distinct peaks were detected in the ^{13}C-NMR. Symmetry considerations and their exceptionally strong intensities suggest that the peaks at 127.6 and 129.7ppm each represent two carbons, adding up to 25 carbons. This leaves one carbon unassigned, which was later revealed to be a quaternary carbon at 137ppm. This last carbon was previously undetected due to the poorly resolved peak at 137ppm, which represented two accidentally degenerate distinct C sites.

IR analysis

The broad peak at 3360.06 cm^{-1} indicates presence of OH groups and is likely to have overlapped with a secondary NH group, which typically appears as a single band at ~3300cm^{-1} [14]. The strong peak at 1690.28cm^{-1} represents a carbonyl, which does not belong to an aldehyde (1740 – 1725cm^{-1}) or ketone (1720 – 1708cm^{-1})[14]. The carbonyl group likely belongs to an amide (C=O stretch at ~1690-1640cm^{-1}) and not an ester (C=O stretch at ~1750-1735cm^{-1}). The absence of a strong C-O stretch signal (typically intense peaks) from 1300-1000cm^{-1} corroborates the absence of an ester. Quinolinones are known to contain amide groups as well, thus the ^{13}C-NMR peak at 168.93ppm represents an amide instead of an ester.

2D-NMR analysis

HSQC analysis allowed for protons to be matched to their respective carbons, as shown in table 1. As only 25 carbons were found from the C-NMR peaks, the last carbon (C26) could have been an unresolved overlapping peak in the C-NMR, which was given as C26 at δ = 137ppm.

C No.	^{13}C Chemical shift (ppm)	^{1}H Chemical shift (ppm)	Type
1	168.93		Q
2	156.74		Q
3	140.41		Q
4	137.04	6.38	CH
5	129.93	7.26	CH
6	129.71	7.26	CH
7	129.71	7.26	CH
8	127.97	7.37	CH
9	127.60	7.26	CH
10	127.60	7.26	CH
11	122.96	6.85	CH
12	122.34		Q
13	112.68		Q
14	108.14	6.45	CH
15	86.30	3.64	CH
16	84.35		Q
17	83.18		Q
18	80.15		Q
19	59.19	3.54	CH_3
20	29.69	1.32	CH_3
21	29.10	1.54	CH
22	27.00	1.82	CH
23	26.44	1.20	CH_3
24	26.24	1.29	CH_3
25	6.57	0.51 (H^a) 0.45 (H^b)	CH_2
26	137		Q

Table 1. Carbons and protons with assigned chemical shifts from C-NMR and HSQC analysis (Q: quaternary)

Analysis of the COSY spectrum allowed for the identification of spin systems, and hence derivation of the fragments in Fig. 17. The COSY showed a strong peak coupling H8 and H14, and since H8 is an aromatic proton, H14 is likely to be adjacent to H8 on the same aromatic ring, producing fragment 1. Fragment 2 was then derived from the H11 coupling to H4. Lastly, the cyclopropane ring (fragment 3) was derived from the coupling of both H22 and H21 to H25 (H^a and H^b), indicating that C25 could be in the middle of both C21 and C22. H22 also coupled with H21, and the only way to accommodate these pairings is a cyclopropane ring.

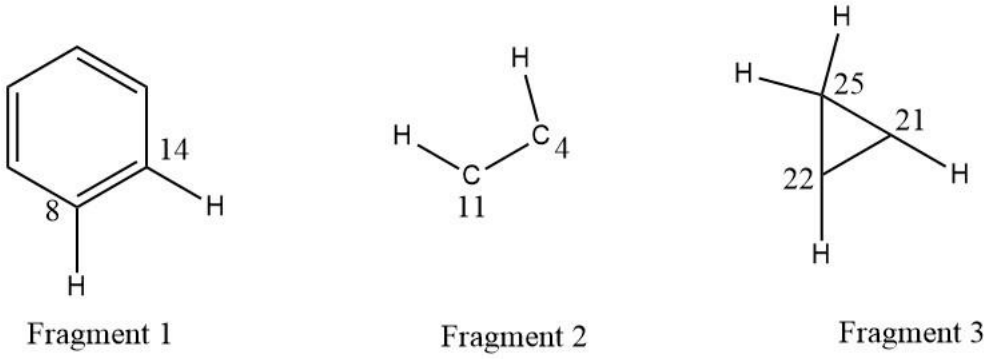

Fig 17. Fragments obtained from COSY analysis

Use of HMBC correlations to piece the COSY-derived fragments together resulted in the final structure (without stereochemistry) shown in Fig. 20. Analysis started from the methyl groups, whereby H20 and H23 both correlated with C17, suggesting that C20 and C23 are connected to C17. H24 → C16, C22, C4, which leads to the possibility of the CH_3 group (C24) being on either C16 or C4. C16 was chosen since C4 has correlations with aromatic protons and is hence of further proximity to H24 than C16. C16 → H4, suggesting that C4 is adjacent to C16, which inserts fragment 2 into the overall molecule. The chemical shifts of H4 and H11 (δ = 6.38, 6.85)

suggests a double bond between C4 and C11. This would result in fragment 4 (Fig. 18). The COSY coupling constant between H4 and H11 ($J_{H4\text{-}H11} \approx 17$Hz) was indicative of a trans double bond (typically 11 – 18Hz).

As there were no correlations between C16 and H20/H23, and C17 and H24, it is likely that there is a heteroatom between C17 and C16 and a ring closure, but this was to be determined after further HMBC analysis of the remaining fragments.

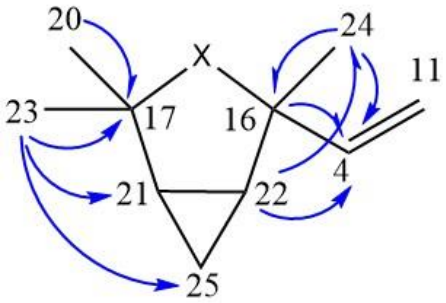

Fragment 4

Fig 18. Fragment 4 derived from HMBC correlations

H4 → only C16, C24, C12 indicates that quaternary C12 is connected to C11. The next step would be to look for HMBC correlations to H11. H11 → C12, C2, C8 which leads to C12 connecting to C2 and C8. This allows for insertion of COSY-derived fragment 1 (containing C8) into the overall molecule, with two remaining unassigned aromatic carbons. H8 → C13, C26 and H14 → C13 showed that the remaining two carbons were C13 and C26. For C2 to be quaternary, it must be connected to a heteroatom or another quaternary carbon. As it has a higher chemical shift ($\delta = 156.74$ppm) than the other carbons in the same aromatic ring, X^2 is likely a heteroatom with de-shielding effects. This allowed for derivation of fragment 5 (Fig. 19).

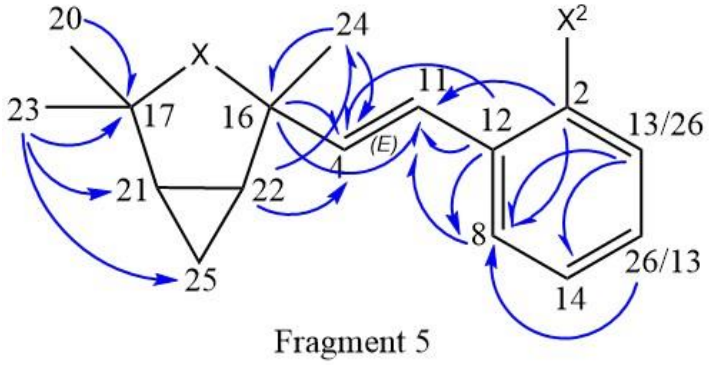

Fig 19. Fragment 5 derived from HMBC correlations

The remaining unassigned methyl group (C19) is likely a methoxy group, considering its chemical shift (H19 δ = 3.54) and its lack of HMBC correlations to other carbons except for C15. The correlation H15 → C1, C18, C13 shows that C15 connects to both C1 and C18, thus determining the position of the amide group in the molecule and the position of C13 as adjacent to C18. At this juncture, there is still a mono-substituted aromatic ring with 5 protons (δ = 7.26ppm) that has not been connected to the overall molecule. Since H15 → C3 and C18 is the only available carbon remaining, the aromatic ring was attached to C18. Lastly, there are still 3 oxygen atoms left unassigned. Inserting hydroxyl groups on C18 and C2 and an O between C16 and C17 would complete the molecular formula and fulfill the aforementioned hints. Closing the ring between C16 and C17 also fulfills the 13 degrees of unsaturation. Using HSQC, COSY and HMBC analysis, the final structure (Fig. 20) was elucidated, and was shown to be a quinolinone alkaloid derivative.

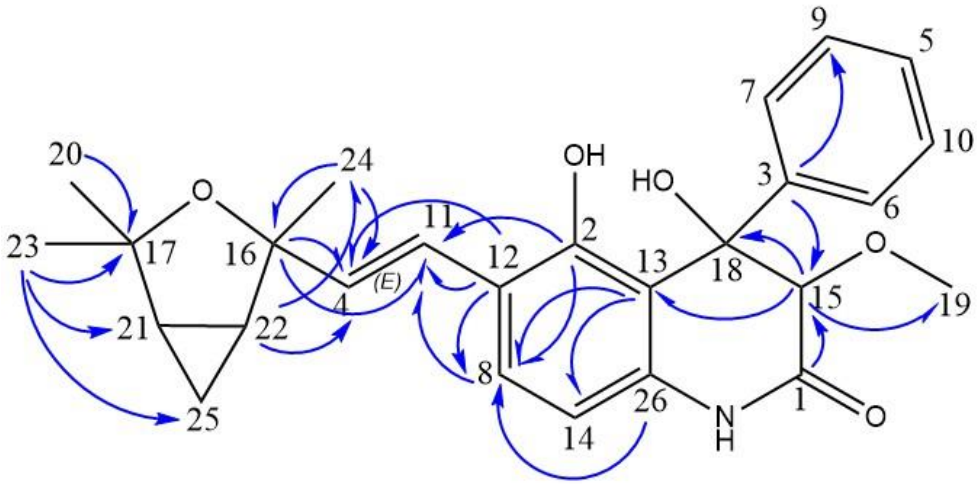

Fig 20. Structure of compound 1 (without stereochemistry assignments)

In order to assign stereochemistry, NOESY analysis was carried out (Fig. 21). H25 (H^b) correlated with both H20 and H24, indicating that they were co-facial. H21, which is anti-facial to H25, correlated with H23, indicating that H21 and H23 are on opposite sides of H25. NOESY, however, could not be used to determine stereochemistry of C15 and C18 due to their isolated location in the molecule and their lack of protons.

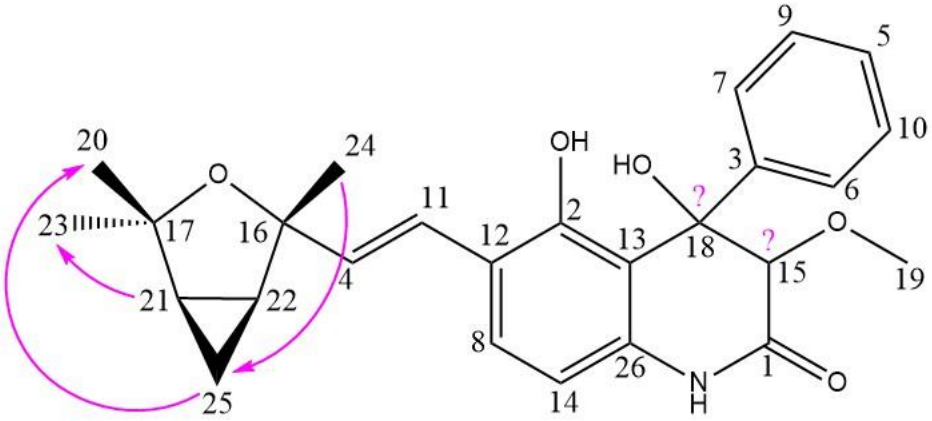

Fig 21. Structure of compound 1 with stereochemistry assigned from NOESY analysis

Determining Stereochemistry by RDCs and ECD

Background RDC Theory

Not all stereocenters can be determined through NOESY NMR due to low degree of protonation, their remote location in the molecule, lack of parametrization of Karplus coefficients or interspin distances that are too large to observe appropriate NOEs[19] (interspin distances beyond 5Å[20] are challenging to detect). Due to the short-range nature of NOESY, one can use residual dipolar coupling (RDC) values as a complementary method to determine relative stereochemistry.

When proximate molecules in a solution are partially aligned, this leads to incomplete averaging of anisotropic dipolar couplings (e.g. magnetic dipole-dipole interactions), resulting in residual dipolar coupling (RDC) between two spins in a molecule[21]. For two nuclear spins j and k, the absolute size of the RDC depends on the distance between two spin nuclei (r_{jk}), the angle (θ_{jk}) between the internuclear vector and the direction of the external magnetic field (B_0), and the gyromagnetic ratios γ of the involved nuclear spins. This results in the following equation (1) [19]:

$$D_{jk} = -\frac{1}{2} \cdot \left(\frac{\mu_0}{8\pi^2}\right) \cdot \frac{\gamma_j \gamma_k \hbar}{r^3{}_{jk}} \langle 3cos^2\theta_{jk} - 1 \rangle$$

whereby the angular brackets represent averaging over time, resulting in scaled dipolar couplings.

Obtaining RDC data

To measure RDCs experimentally, one can conduct t_2-coupled ^{1}H-^{13}C HSQC in the presence (anisotropic) and in the absence (isotropic) of an orienting media[22]. The $^1J_{CH}$ couplings and total couplings ($^1T_{CH}$) are measured in the isotropic and

anisotropic media respectively, and RDC values ($^1D_{CH}$) can be calculated by equation (2) [22]:

$$^1D_{CH} = {}^1T_{CH} - {}^1J_{CH}$$

In the case where RDCs are too small, this method is less reliable. Instead, one may superimpose the isotropic and anisotropic HSQC spectra based on their peak shapes. The exponential apodization function may also be used for a better fit in cases of different spectral patterns.

It should be noted that sensitivity and resolution of the ^1H spectrum can be highly compromised by the alignment media. For example, the use of media such as PBLG (poly-γ-benzyl-L-glutamate) aligns molecules too strongly, causing significant line broadening and hence compromising resolution[22]. Instead, Griesinger et al. uses a copolymeric crosslinked polyacrylamide (PH gel) that is compatible with commonly used solvent DMSO and greatly reduces the line broadening effect, maintaining good resolution. Greisinger has proven the reliability of PH gel in experiments with (+)-menthol[22], producing well-resolved spectrums in suitable solvents. The slim PH-gel is usually prepared for a 1.7mm NMR tube to acquire the RDC data. This method is suitable for limited amounts of sample.

Analysis of RDCs and ECD

Upon obtaining RDCs experimentally in PH gel, theoretical RDC values must be obtained for comparison. To predict theoretical RDCs, the Singular Value Decomposition (SVD) method is used to calculate an alignment tensor (requires at least 5 RDC values) for each possible conformation[23]. Then, the experimental RDC is fitted to the theoretical RDCs back-calculated from the alignment tensors and the quality of the fitting is expressed by the Cornilescu quality factor Q (Q = rms (D^{exp}

– D^{calc})/rms D^{exp}) [20]. The theoretical structure with the lowest Q value is the correct structure.

Since three out of the five stereocenters in Fig. 6 have already been determined by NOESY, there are only four final possible configurations – RRSRR, RRSRS, and their enantiomers (RRSSS and RRSSR) for C16, C21, C22, C15 and C18 respectively. The two configurations (RRSRR and RRSRS) are optimized and their theoretical RDCs are predicted through the SVD method, while experimental RDC for the unknown alkaloid is determined through equation (2). By comparing the experimental and theoretical RDCs, Q factors can be derived and the diastereomer with the lowest Q factor corresponds to the correct relative configuration.

To determine absolute configuration, electronic circular dichroism (ECD) may be used. Time dependent density functional theory (TDDFT) calculations can be used to generate theoretical ECDs[24]. The B3LYP/6-31G functionals and basis set has been proven to be a reliable choice for TDDFT calculations[24]. The experimental ECD can be measured using commercial ECD spectrometers operating in the UV-Vis spectral region. The experimental and theoretical ECD spectra will then be superimposed, presented as differential molar extinction ($\Delta\varepsilon$) as a function of wavelength (λ). By comparing the experimental and theoretical ECD spectra and observing how closely they match, the absolute configuration of the unknown alkaloid can be determined. For example, if the RRSRR diastereomer was correct according to the RDCs, a theoretical ECD should be generated for both the RRSRR and RRSSS enantiomer. The experimental ECD will reproduce the signs and the shape of the theoretical ECD for the correct enantiomer[23]. If necessary, the

experimental ECD can be red- or blue-shifted to fit the theoretical ECDs better, since TDDFT calculations might over- or under-estimate excitation energy[23].

Improving resolution of ^{13}C-NMR

While there were 26 carbons in the unknown molecule, the ^{13}C-NMR (Fig. S3) only showed 23 peaks, with an overlapped peak at 137ppm preventing identification of the quaternary carbon at 137ppm, showing that resolution can further be improved. Poor resolution may be due to short acquisition time (at). Since spectral resolution = 1/at [16], an increase in at may improve spectral resolution. However, this will not work if peaks are already broad, implying short FID and hence sufficient at. The absence of the quaternary carbon peak at 137ppm could also be due to low signal-to-noise ratio. Since signal-to-noise ratio improves with $nt^{1/2}$, one should consider increasing the number of scans (nt). However, it should be noted that increasing the number of scans infinitely is impractical and time-consuming. Finally, a spectrometer of higher field strength and hence better resolution can be used e.g. 600MHz for ^{1}H-NMR and 150MHz for ^{13}C-NMR. While a solvent change may be considered, the polar solvent CD_3OD used should have been able to solvate the polar alkaloid relatively well.

Resolving Ambiguities in Structure Elucidation

While alternative structures such as AS1 (Fig. 22) were considered, they were mostly ruled out by HMBC correlations. It was possible that C18 was connected to C26 and the amide group adjacent to C13 to produce AS1. However, the presence of HMBC correlation C13 → H15 and absence of C26 → H15 confirmed that AS1 was unlikely compared to the decided final structure.

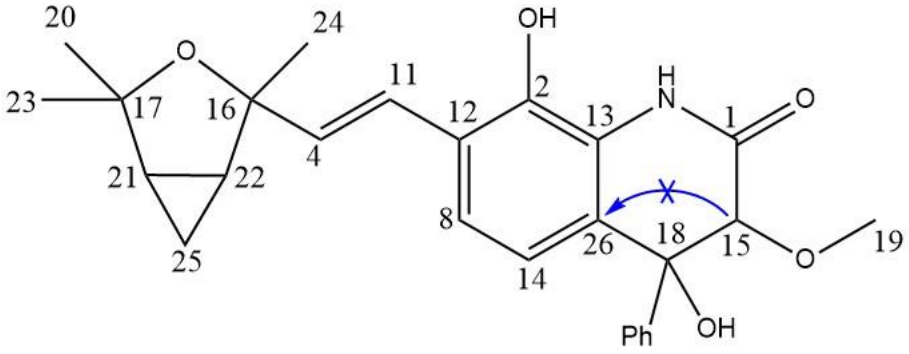

Fig 22. Alternative structure 1 (AS1)

Conclusion

Natural products extracted from fungi can be classified into many classes – aromatic compounds, amino acids, anthracenones, butanolides, butenolides, cytochalasans, napthalenones, terpenes[25-26], quinolinones and others. Of these, a few are known to exhibit anti-cancer properties, although research efforts have not led to an established fungi-derived clinical cancer drug yet. Such fungi-derived natural products include analogues of Fumagillin (of *Aspergillus fumigatus*) which have been tested in human cancer clinical trials for their ability to disrupt tumor vasculature[27], Rhizoxin (of *Rhizopus chinensis*) which binds to tubulin to inhibit microtubule assembly[28], Aphidicolin (of *Cephalosporium aphidicola*) which is a specific inhibitor of DNA polymerases α and δ[29]; and Tryprostatins A and B (of *Aspergillus Fumigatus)*which is an inhibitor of mitogen activated protein (MAP)-kinase-dependent microtubule assembly[30].

Likewise, anti-cancer properties of compound 1 in this work may be discovered through common bioassays. Typically, one would compare the anti-cancer activity of the experimental drug (compound 1) to a standard anti-cancer drug by testing them on a cancer cell line and a control cell line (non-malignant). Cytotoxicity

parameters e.g. IC50, IC90 and LC50 may then be obtained through cytotoxicity tests (e.g. SRB, MTT assays[31]) for both drugs in both cell lines. In vivo tests may also be carried out to analyze therapeutic efficacy and toxicity, measuring parameters such as mice weight loss, overall survival rate etc.

In summary, despite the rarity of fungal-derived natural products approved for clinical use, it is likely that an effective drug will be discovered in time, as cytotoxicity-testing methods and structure elucidation techniques improve.

Spectral Data

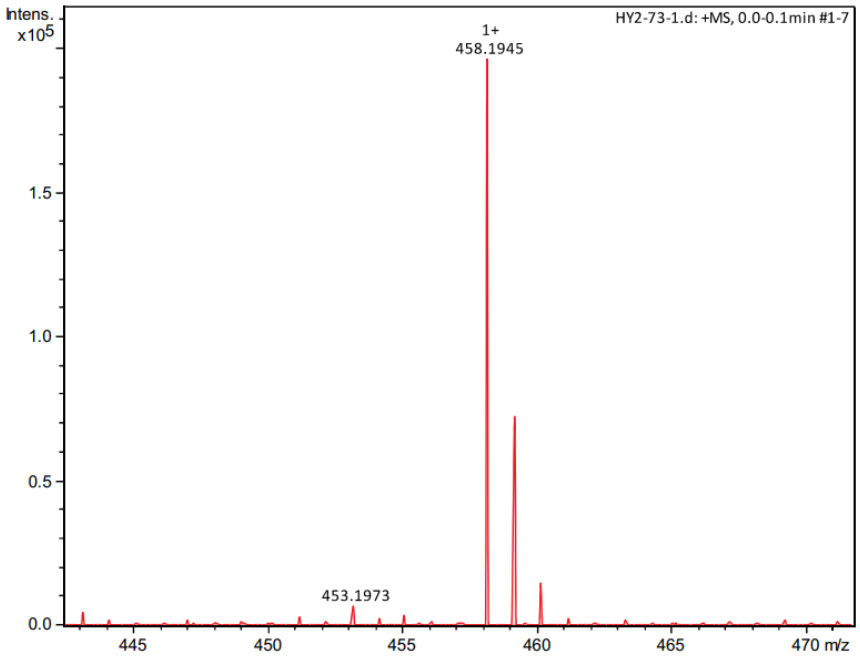

Figure S1. HRESIMS spectrum of compound **1**

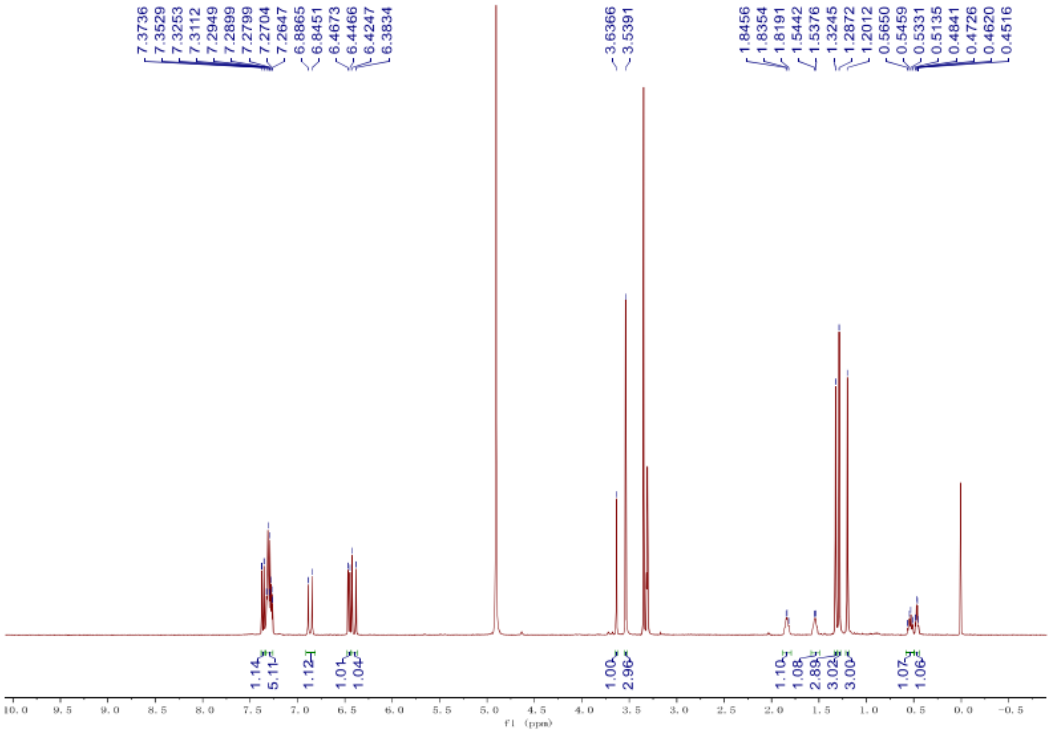

Figure S2. ^{1}H NMR of compound **1** (CD_3OD, 400MHz)

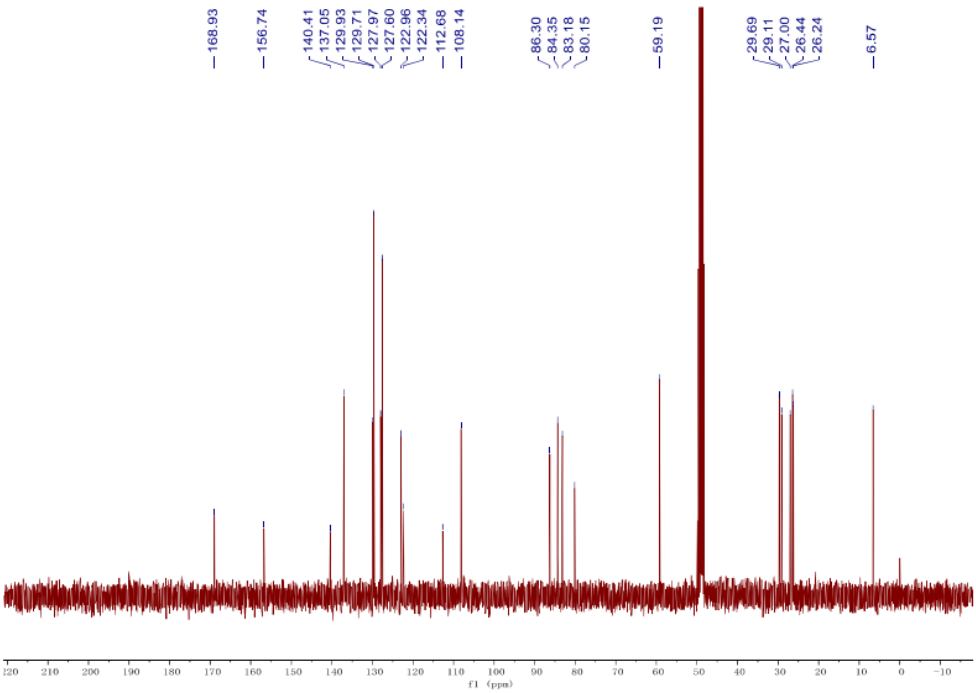

Figure S3. ^{13}C NMR of compound **1** (CD_3OD, 100MHz)

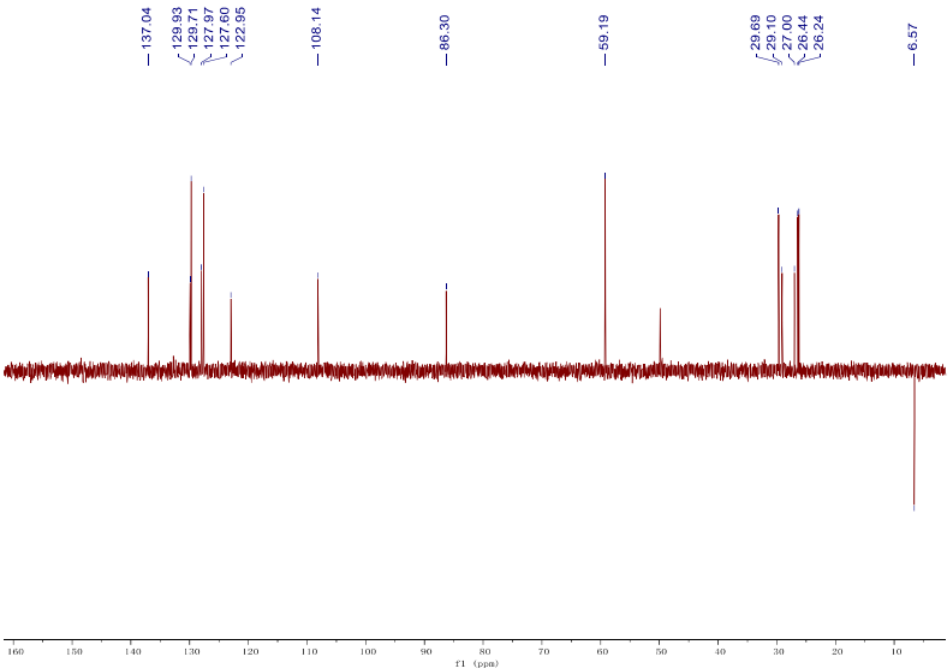

Figure S4. DEPT spectrum of compound **1** (CD_3OD, 100MHz)

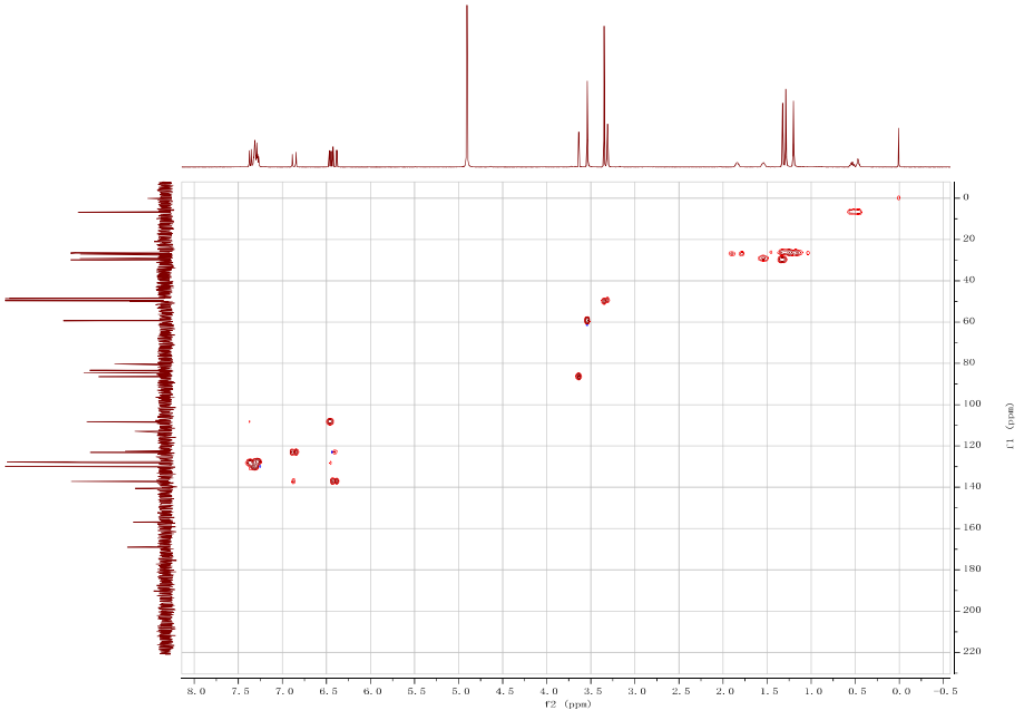

Figure S5. HSQC spectrum of compound **1** (CD_3OD, 400MHz)

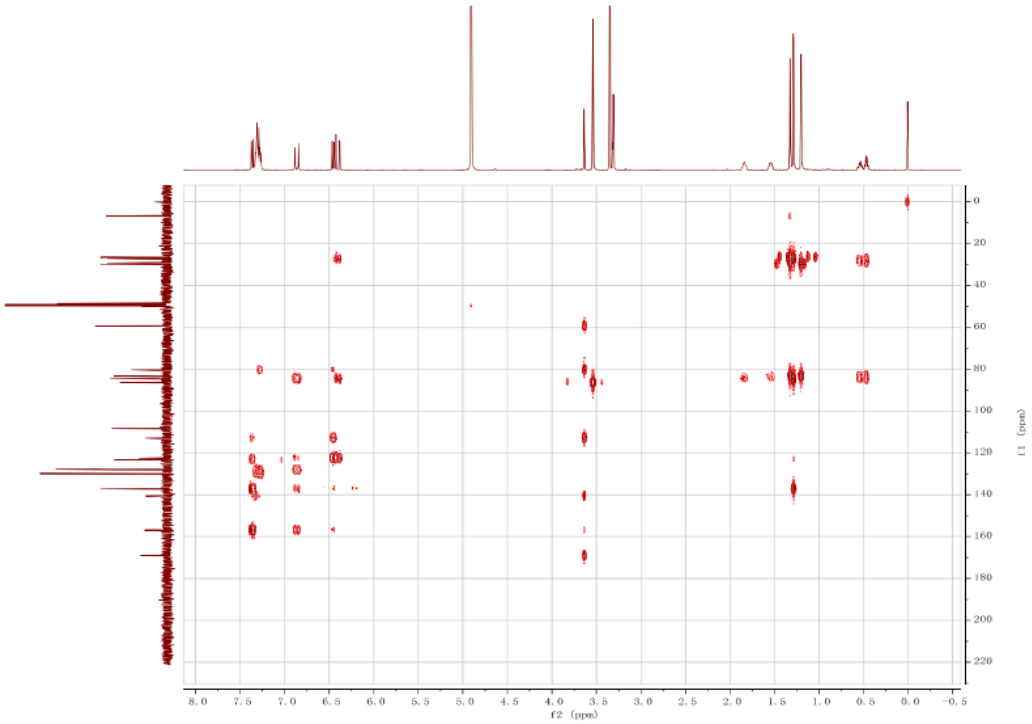

Figure S6. HMBC spectrum of compound **1** (CD_3OD, 400MHz)

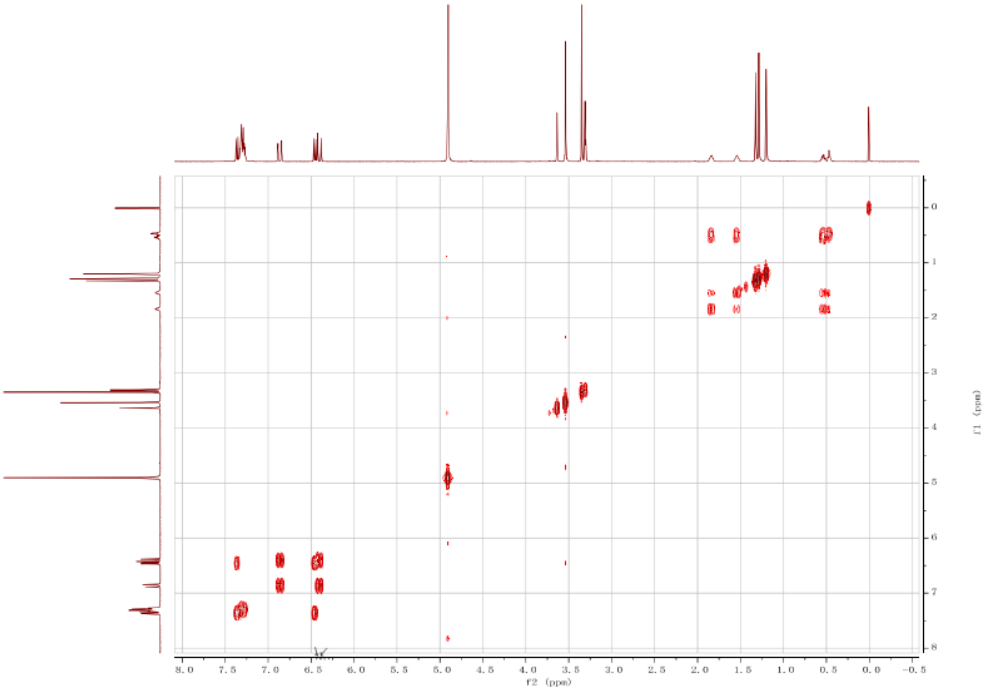

Figure S7. ^{1}H-^{1}H COSY spectrum of compound **1** (CD_3OD, 400MHz)

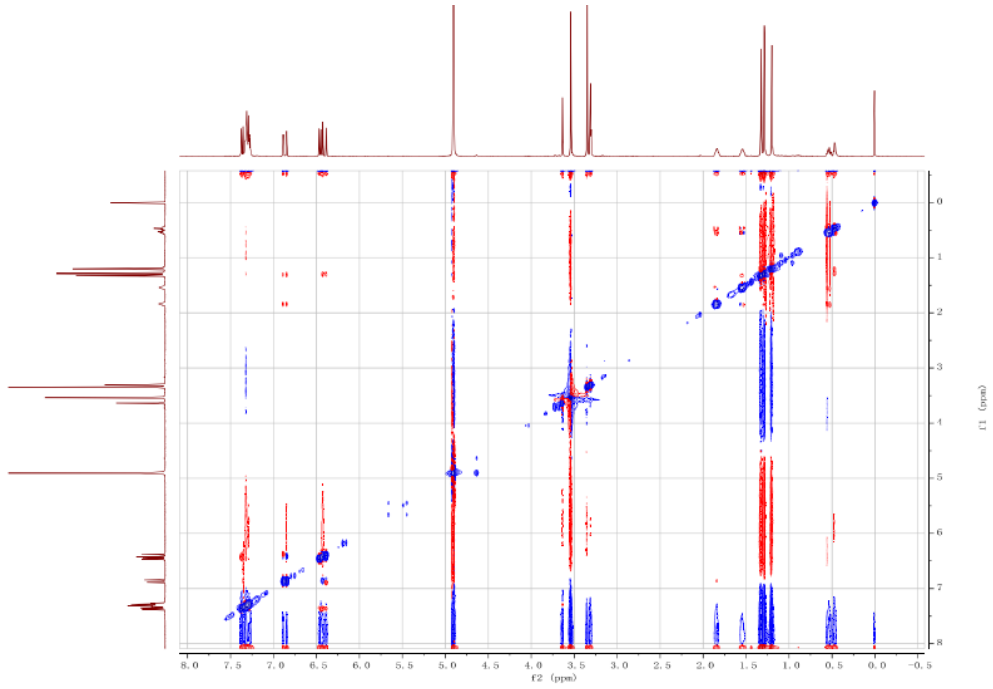

Figure S8. NOESY spectrum of compound **1** (CD_3OD, 400MHz)

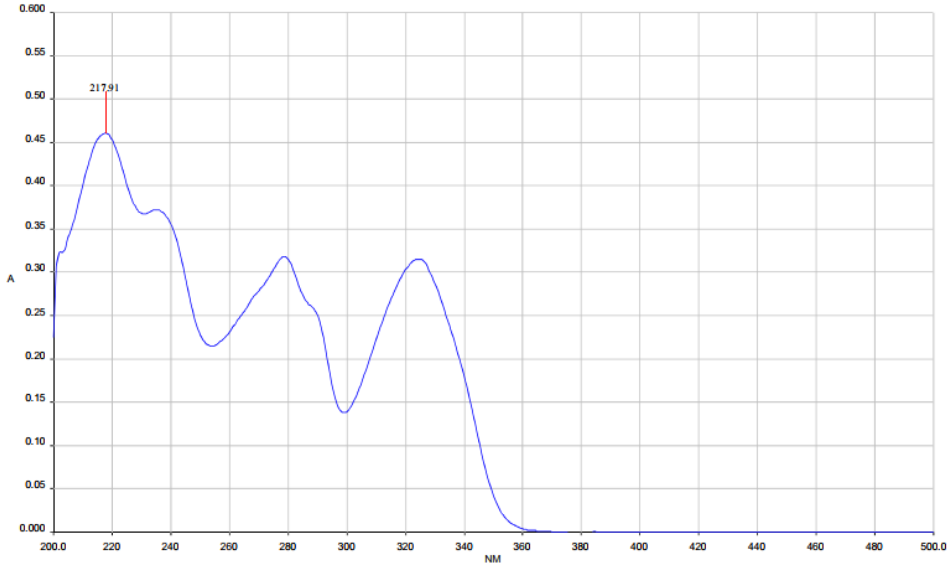

Figure S9. UV spectrum of compound **1**

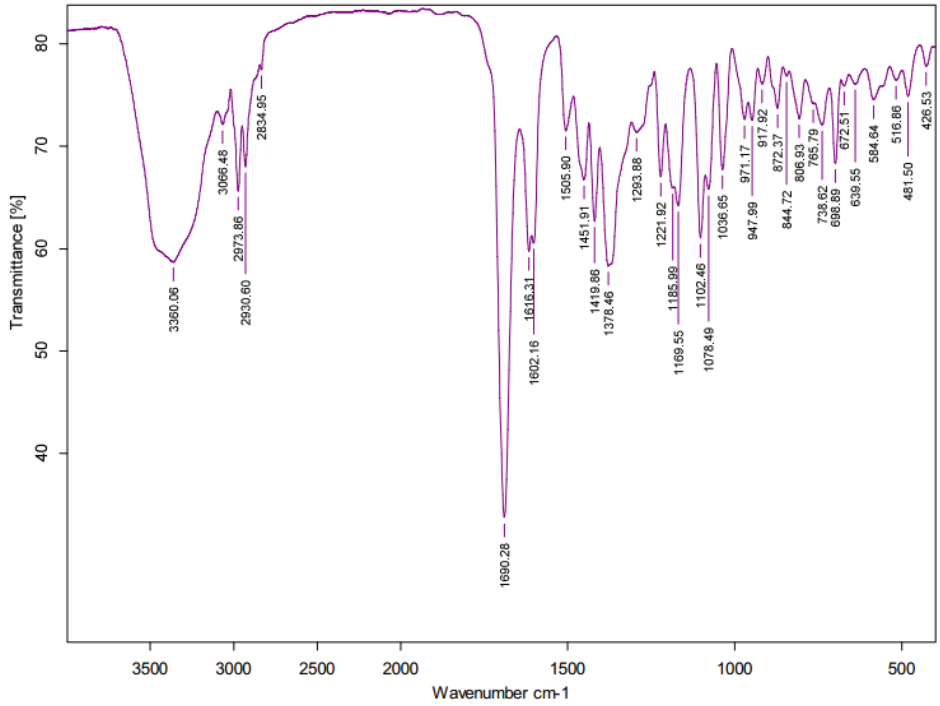

Figure S10. IR spectrum of compound **1**

References

1. D. Jakubczyk et al. Selected Fungal Natural Products with Antimicrobial Properties. *Molecules.* 2020, 25(4), 911.
2. R. Kiss et al. Towards a Cancer Drug of Fungal Origin. *Med Res Rev.* 2015, 35(5), 937-967.
3. S. Ruchirawat et al. Alkaloids as Important Scaffolds in Therapeutic Drugs for the Treatments of Cancer, Tuberculosis, and Smoking Cessation. *Current Topics in Med. Chem.* 2014, 14(2), 239-252.
4. T. P. T. Cushnie et al. Alkaloids: An Overview of their Antibacterial, Antibiotic-enhancing and Antivirulence Activities. *Int J. Antimicrobial Agents.* 2014, 44(5), 377-386.
5. M. Zhang et al. Cytotoxic Alkaloids and Antibiotic Nordammarane Triterpenoids from the Marine-Derived Fungus *Aspergillus sydowi. J. Natural Products.* 2008, 71(6), 985-989.
6. A. Broberg et al. Antibacterial Isoquinoline Alkaloids from the Fungus *Penicillium Spathulatum* Em19. *Molecules.* 2019, 24(24), 4616.
7. I. Vaca et al. Filamentous Fungi from Extreme Environments as a Promising Source of Novel Bioactive Secondary Metabolites. *Front Microbiol.* 2015, 6, 903.
8. D. Tasdemir. Marine Fungi in the Spotlight: Opportunities and Challenges for Marine Fungal Natural Product Discovery and Biotechnology. *Fungal Biology and Biotechnology.* 2017, 4(5).
9. K. Scherlach et al. Aspernidine A and B, Prenylated Isoindolinone Alkaloids from the Model Fungus *Aspergillus Nidulans. The J. Antibiotics.* 2010, 63, 375-377.

10. Q. Liu et al. Genome Mining and Biosynthesis of a Polyketide from a Biofertilizaer Fungus that can Facilitate Reductive Iron Assimilation in Plant. *PNAS.* 2019, 116(12), 5499-5504.
11. C. C. C. Wang et al. Asperfuranone from *Aspergillus Nidulans* Inhibits Proliferation of Human Non-Small Cell Lung Cancer A549 Cells via Blocking Cell Cycle Progression and Inducing Apoptosis. *Basic & Clinical Pharmacology & Toxicology.* 2010, 107(1), 583-589.
12. C. W. K. Lam et al. Electrospray Ionisation Mass Spectrometry: Principles and Clinical Applications. *Clin Biochem Rev.* 2003, 24(1), 3-12.
13. S. Banerjee et al. Electrospray Ionization Mass Spectrometry: A Technique to Access the Information beyond the Molecular Weight of the Analyte. *Int J Anat Chem.* 2012, 8.
14. D. L. Pavia et al. (2008). *Introduction to Spectroscopy.*
15. D. L. Pavia et al. (2009). *Spectroscopy.*
16. Claridge D. W. (1999). *High-Resolution NMR Techniques in Organic Chemistry.*
17. Separation Science. Dealing with Metal Adduct Ions in Electrospray: Part 1. Available at https://learning.sepscience.com/hubfs/Technical%20Blogs/MS_Sol_3.pdf
18. M. Stojanović et al. ^{1}H NMR Chemical Shifts of Cyclopropane and Cyclobutane: A Theoretical Study. *J. Org. Chem.* 2013, 78(4), 1504-1507.
19. C. M. Thiele et al. Determining the Stereochemistry of Molecules from Residual Dipolar Couplings (RDCs). *eMagRes.* 2012, 1, 169-180.
20. X. X. Lei et al. Residual Dipolar Couplings in Structure Determination of Natural Products. *Natural Products and Bioprospecting.* 2018, 8, 279-295.

21. E. Brunner. Residual Dipolar Couplings in Protein NMR. *Concepts in Magnetic Resonance.* 2001, 13(4), 238-259.
22. C. Griesinger et al. A DMSO-Compatible Orienting Medium: Towards the Investigation of the Stereochemistry of Natural Products. *Angew. Chem. Int. Ed.* 2005, 44, 427-429.
23. C. Griesinger et al. The Use of a Combination of RDC and Chiroptical Spectroscopy for Determination of the Absolute Configuration of Fusariumin A from the Fungus *Fusarium* sp. 2016, 6, 41-48.
24. X. Li et al. Determination of Absolute Configuration of Natural Products: Theoretical Calculation of Electronic Circular Dichroism as a tool. *Curr Org Chem.* 2010, 14(16), 1678-1697.
25. W. B. Turner et al. Fungal Metabolites II. *J. Pharm. Sci.* 1984, 73(12).
26. P. M. Dewick. (2009). *Medicinal Natural Products: A Biosynthetic Approach, 3rd Edition.*
27. C. C. Arico-Muendel et al. Carbamate Analogues of Fumagillin as Potent, Targeted Inhibitors of Methionine Aminopeptidase-2. *J Med Chem.* 2009, 52(24), 8047-56.
28. H. L. McLeod et al. Multicentre Phase II Pharmacological Evaluation of Rhizoxin. Eortc Early Clinical Studies (ECSG)/pharmacology and Molecular Mechanisms (PAMM) Groups. *Br. J. Cancer.* 1996, 74(12), 1944-8.
29. C. Sessa et al. Phase I and Clinical Pharmacological Evaluation of Aphidicolin Glycinate. *J. Natl. Cancer. Inst.* 1991, 83(16), 1160-4.
30. T. Usui et al. Tryprostatin A, a Specific and Novel Inhibitor of Microtubule Assembly. *Biochem J.* 1998, 333(3), 543-548.
31. J. McCauley et al. Bioassays for Anticancer Activities. *Methods Mol Biol.* 2013, 1055, 191-205.